

# Reaction mechanisms in the scattering of ${}^8\text{Li}$ on ${}^{208}\text{Pb}$ around the Coulomb barrier

A. M. Moro\* and R. Crespo

*Departamento de Física, Instituto Superior Técnico, 1049-001 Lisboa, Portugal*

H. García-Martínez, E. F. Aguilera, and E. Martínez-Quiroz

*Departamento del Acelerador, ININ, Apartado Postal 18-1027, Caixa Postal 11801, México D.F., Mexico*

J. Gómez-Camacho

*Departamento de FAMN, Universidad de Sevilla, Apartado Postal 1065, 41080 Sevilla, Spain*

F. M. Nunes

*National Superconducting Cyclotron Laboratory, MSU, East Lansing, Michigan 48824-1312, USA*

(Received 18 March 2003; published 30 September 2003)

We present an analysis of the reaction  ${}^8\text{Li}+{}^{208}\text{Pb}$ , which has been recently measured at energies around the Coulomb barrier. The study is focused on the elastic and one-neutron removal channels. The elastic angular distribution has been analyzed by means of the optical model and coupled-channels method. The measured  ${}^7\text{Li}$  yield has been assumed to come from the one-neutron transfer reaction  ${}^{208}\text{Pb}({}^8\text{Li}, {}^7\text{Li}){}^{209}\text{Pb}$  and the breakup reaction  ${}^8\text{Li}+{}^{208}\text{Pb}\rightarrow n+{}^7\text{Li}+{}^{208}\text{Pb}$ . For the former, an analysis in terms of the distorted wave Born approximation and coupled-channels Born approximation (CCBA) methods has been performed. For the breakup reaction, a generalization of the CCBA method has been used, in which the final states are described as  $n+{}^{208}\text{Pb}$  continuum states. Transfer and breakup are then treated consistently. The summed angular distribution for the two processes reproduces the shape and absolute magnitude of the measured  ${}^7\text{Li}$  distribution. We conclude that most of the measured  ${}^7\text{Li}$  yield comes from the one-neutron transfer channel. We also show that the elastic scattering is notably affected by the strong coupling to transfer channels.

DOI: 10.1103/PhysRevC.68.034614

PACS number(s): 24.10.Eq, 24.50.+g, 25.60.Je

## I. INTRODUCTION

From the experience gained with stable nuclei, it is general knowledge that physical phenomena measurable at energies well above the Coulomb barrier may differ significantly from those that are revealed around and below the barrier. Indeed, some effects can be suppressed/enhanced and, furthermore, new phenomena may appear. Recent investigations prove that dripline nuclei show similar effects.

In recent years, a few *small scale* facilities have invested large efforts in measuring reactions with light radioactive beams. In the *larger facilities*, radioactive beams are obtained from the fragmentation of very energetic primary beams of stable nuclei, producing secondary beams with energies of several tens of MeV per nucleon. Counteracting, the unstable nuclei produced in the smaller facilities need to be postaccelerated. Even though these beams are energetically limited to a few MeV per nucleon, their focus and energy are accurately controlled. The analysis of low energies reactions has provided information on the structure of light dripline nuclei and the reaction process, complementary to the high energy regime data.

The multiple measurements of fusion with light exotic nuclei demonstrates the vivid activity in this field. The problem that has been addressed by many authors concerns the role of the halo nucleon(s) when halo nuclei fuse: is there suppression or enhancement of the cross section? This prob-

lem has been object of exhaustive analyses, be it for  ${}^6\text{He}$ ,  ${}^{11}\text{Be}$ , or  ${}^{11}\text{Li}$  [1–9]. However, the controversy raised over a decade ago still subsists. Clarifications, both from the experimental and theoretical point of view, are needed [10].

Other representative examples of recent low energy studies concern measurements of transfer or breakup of  ${}^6\text{He}$ . Such measurements have been performed at Notre-Dame with a  ${}^{209}\text{Bi}$  target, at energies around and below the barrier. By a simultaneous analysis of the elastic, fusion, and transfer/breakup measured cross sections, Aguilera *et al.* [11,12] found that the latter mechanism accounts for basically all the reaction cross section at energies below the barrier. This distinctive feature is probably a direct consequence of the weak binding of the halo neutrons. For a better understanding of this phenomenon, it is desirable to perform similar studies on other systems with weakly bound nucleons.

Additionally, the relatively strong coupling to direct reaction channels at energies below the barrier observed in processes with weakly bound nuclei has been put forth as the principle reason for the apparent absence of the threshold anomaly in these systems [13]. Nevertheless, the scarce experimental data prevents us from making strong conclusions on the generality of these results.

Within this context, there has been a revival of studies involving the Li isotopes. Comparative measurements on  ${}^6\text{Li}$  and  ${}^7\text{Li}$  have been performed in Florida state [14] as well as in São Paulo [15]. These two isotopes exhibit rather different  $\alpha$ -breakup thresholds, thus a consistent theoretical description is by no means trivial.

Apart from any experimental consideration, the study of

\*Email address: moro@nucl.eus.es

low energy reactions with exotic nuclei is certainly challenging from the theoretical point of view. In many situations, a good understanding of the physics requires the use of few-body models beyond those presently available. The main reason being that, at low energy, many of the high energy approximations that simplify the theoretical treatments (classical trajectories, sudden or adiabatic assumptions, multiple scattering expansions, etc.) are no longer valid. In this way, the analysis of low energy reactions also constitute a test on existing methods and a motivation for new developments.

In a recent experiment performed at Notre-Dame, the scattering of  $^8\text{Li}$  on  $^{208}\text{Pb}$  was measured at energies around the Coulomb barrier. The most distinctive feature was a prominent  $^7\text{Li}$  group measured at the incident energies  $E_{\text{c.m.}} = 32.9$  MeV and  $E_{\text{c.m.}} = 33.4$  MeV. Since only charged particles were detected, it was not possible to determine the fate of the removed neutron, and both breakup and transfer contributions need to be considered. Along with this strong  $^7\text{Li}$  group, large cross sections were also found for  $^4\text{He}$  particles at the same energies.

In this work we extend the analysis performed in Ref. [16] in order to obtain a consistent description of the elastic and one-neutron removal channels. For this purpose, we first study the elastic angular distributions, in order to obtain a good description of the entrance channel. An optical model analysis is performed on the elastic angular distributions, providing a set of optical potential parameters for each scattering energy. Since the energy resolution of the cited experiment did not permit the separation of the elastic scattering from the inelastic scattering leading to  $^8\text{Li}$  in the  $E_x = 0.98$  MeV excited state, we have also performed a coupled-channels (CC) analysis of the data, in which both states are explicitly considered and coupled together to all orders. This approach allows the extraction of the elastic and inelastic contributions to the  $^7\text{Li}$  yield, within the uncertainties of the model.

The measured  $^7\text{Li}$  is inclusive with respect to the transferred neutron. From the various processes that could, in principle, contribute, we restrict our analysis to the direct transfer of the valence neutron to the bound states of  $^{209}\text{Pb}$  and the breakup of the projectile to continuum states. Second or higher order terms involving projectile or target excitation besides the one-neutron removal are ignored, since they are expected to have a small effect on the inclusive cross sections. In our calculations, breakup is treated as transfer of the valence neutron to the target continuum. The treatment of breakup as transfer to continuum excited states of the target has been recently applied to study the Coulomb dissociation of one-neutron halo nuclei on heavy targets [17,18]. Also, a similar method has been developed by Bonaccorso and Brink [19] to study nucleon transfer reactions at medium and high energies, using a semiclassical model.

The paper is organized as follows. In Sec. II, the quasi-elastic angular distributions are analyzed within the optical model and coupled-channels frameworks. In Sec. III, we analyze the transfer channels within the distorted wave Born approximation (DWBA) and coupled-channels Born approximation (CCBA) schemes. In Sec. IV, a similar analysis

TABLE I. Optical potential parameters used in the calculations at  $E_{\text{c.m.}} = 33.1$  MeV. The Coulomb parameter for  $^7,8\text{Li} + ^{208}\text{Pb}$  is  $r_C = 1.25$  fm. For each potential, the reduced radius is the same for all the real, imaginary, and spin-orbit parts. This radius has to be multiplied by  $A_t^{1/3}$  for nucleon-nucleus potentials and  $A_p^{1/3} + A_t^{1/3}$  for the  $^7,8\text{Li} + ^{208}\text{Pb}$  potentials. The spin-orbit term refers to the binding potentials.

System	$V_0$	$r_x$	$a_0$	$W_0$	$a_i$	
$^7\text{Li} + ^{208}\text{Pb}$	15.4	1.3	0.65	13.2	0.65	Reference [20]
$^8\text{Li} + ^{208}\text{Pb}$	15.4	1.3	0.65	58.4	0.70	OM-1
$^8\text{Li} + ^{208}\text{Pb}$	37.1	1.3	0.65	154	0.57	OM-2
$^8\text{Li} + ^{208}\text{Pb}$	60.0	1.3	0.65	154	0.60	CC
$^8\text{Li} + ^{208}\text{Pb}$	60.0	1.3	0.65	154	0.55	CRC
System	$V_0$	$r_0$	$a_0$	$V_{ls}$	$a_{ls}$	
$n + ^7\text{Li}$	BE <sup>a</sup>	1.25	0.52	4.89	0.52	Reference [22]
$n + ^{208}\text{Pb}$	BE	1.25	0.65	7	0.65	

<sup>a</sup>Depth adjusted to give the binding energy (BE).

is performed for the breakup channel. The effect of higher order terms in the transfer channels is studied in Sec. V. Finally, Sec. VI includes a brief summary and the conclusions of our work.

## II. ANALYSIS OF THE ELASTIC SCATTERING

### A. Optical model analysis

The study of the elastic scattering  $^8\text{Li} + ^{208}\text{Pb}$  gives a valuable information about the interactions between the colliding nuclei and may provide insight into the relevance of nonelastic channels through the deviation with respect to Rutherford scattering.

In the experiment under study, elastic angular distributions were measured at several incident energies ranging from  $E_{\text{c.m.}} = 24.4$  MeV to  $E_{\text{c.m.}} = 33.1$  MeV. Following the standard procedure, we have performed an optical model analysis of these distributions. The optical potentials were parametrized in terms of usual Woods-Saxon forms, with real and imaginary volume parts. The initial parameters were taken from the optical potential reported in Ref. [20] that describes the  $^7\text{Li} + ^{208}\text{Pb}$  elastic scattering at  $E_{\text{lab}} = 33$  MeV. The calculations were performed with the computer code FRESKO [21], version frxy. In order to permit a comparison between  $^7\text{Li}$  and  $^8\text{Li}$ , we tried to vary as few parameters as possible. We found that fixing the imaginary diffuseness to  $a_i = 0.7$  fm, and taking the imaginary depth as the only free parameter, a good overall fit of the data could be achieved. The optimal parameters for the data at  $E_{\text{c.m.}} = 33.1$  MeV (potential OM-1) are listed in Table I. The resulting angular distribution is given by the dashed line in Fig. 1.

Indeed, if more parameters are allowed to vary, better fits of the data can be obtained. For instance, a very good fit of the distribution for  $E_{\text{c.m.}} = 33.1$  MeV can be achieved by allowing the depths and the imaginary diffuseness to vary. The resulting potential, denoted by ‘‘OM-2,’’ is also listed in Table I. This optical potential provides a better fit at large angles than the previous one (OM-1), as can be noticed via

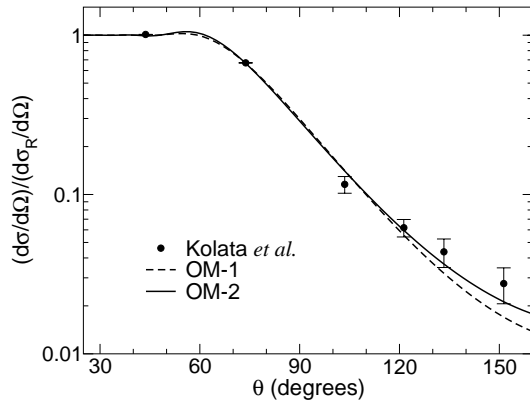


FIG. 1. Elastic cross section angular distributions for the scattering  ${}^8\text{Li}+{}^{208}\text{Pb}$  at  $E_{c.m.}=33.1$  MeV. The dashed and solid lines correspond to optical model calculations performed with parameters OM-1 and OM-2 from Table I.

sually in Fig. 1. However, this improvement on the quality of the fit requires a very deep imaginary potential. Despite their different shape, both potentials indicate a strongly absorptive nature of the  ${}^8\text{Li}$  scattering, which is evidenced in either the large imaginary diffuseness (as compared to the real one) or the very deep imaginary potential. Interestingly, the same conclusion holds for the other energies of the experiment. These results suggest that nonelastic channels are more important in the case of  ${}^8\text{Li}$  scattering as compared to the  ${}^7\text{Li}$  case. A more detailed discussion on this result can be found in Ref. [24].

### B. Coupled-channels analysis

The energy resolution of the present experiment was insufficient to separate the elastic scattering from the inelastic scattering leading to the  $1_1^+$  excited state ( $E_x=0.98$  MeV) of  ${}^8\text{Li}$ . This means that the angular distributions analyzed in the preceding section actually correspond to quasielastic scattering rather than pure elastic scattering. In order to separate the elastic from the inelastic data and to gain a better understanding of these quasielastic data, we performed a CC calculation, in which the entrance channel is described in a two-state model space, including the ground and the first excited state. These states were coupled to all orders. In order to generate the coupling potentials, a collective model for the  ${}^8\text{Li}$  nucleus was assumed. Coulomb and nuclear matrix elements were obtained from the experimental value of the reduced transition probability  $B(E2)$  and the deformation length  $\delta$ , respectively. In particular, we adopted the values  $B(E2)=30 e^2 \text{fm}^4$  and  $\delta=1.75$  fm, derived in Ref. [25]. Besides the nondiagonal terms, diagonal couplings were also considered, in order to account for the reorientation of the projectile. The diagonal matrix elements were obtained from the nondiagonal matrix elements, assuming that the  $2_1^+$  and  $1_1^+$  states belong to a  $K=1$  rotational band, as done in Ref. [25]. For the central potential, we took as initial parameters those for the optical potential OM-2 derived above. Due to the explicit inclusion of the  $1_1^+$  state in the calculation, this optical potential produces an overestimation of the data at all

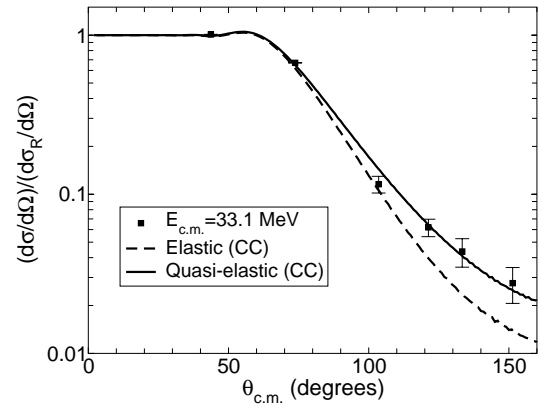


FIG. 2. Quasielastic cross section angular distributions (as ratio to Rutherford) for the scattering  ${}^8\text{Li}+{}^{208}\text{Pb}$  at  $E_{c.m.}=33.1$  MeV. The curves correspond to a coupled-channel analysis using the optical potential “CC” of Table I.

angles. We found that the agreement with the data can be restored by increasing the depth of the real part of the optical potential and the imaginary diffuseness. We show in Fig. 2 the quasielastic cross section angular distribution for the data at  $E_{c.m.}=33.1$  MeV using a modified OM-2 optical potential, in which the imaginary diffuseness was set to  $a_i=0.60$  fm and the real depth was increased to  $V_0=60$  MeV (potential “CC” hereafter). The thick solid line corresponds to the sum of the elastic and inelastic cross sections while the dashed line is the elastic contribution. By comparison of the two curves, we observe that there is a significant contribution of the inelastic cross section in the quasielastic data, particularly at backward angles. As in the optical model analysis, we notice that the optical potential still requires a strongly absorptive part.

Qualitatively similar results are obtained by starting with the set of parameters “OM-1.” In this case, the quasielastic data are well reproduced by increasing the imaginary depth to  $W_0=80$  MeV.

### III. ONE-NEUTRON TRANSFER

As mentioned in the Introduction, the most remarkable finding of the present experiment is the large cross section associated to the  ${}^7\text{Li}$  yield, coming from one-neutron transfer to the target and/or  ${}^8\text{Li}$  breakup. Since the measurements presented in Ref. [16] are inclusive with respect to the residual nucleus and the removed neutron, the experimental data by themselves does not permit to separate both contributions. For this reason, the mechanism producing the measured  ${}^7\text{Li}$  in the present reaction is referred to in Ref. [16] as transfer/breakup. One of the purposes of the present work is to disentangle the relative importance of both mechanisms and to verify that the sum of their cross sections accounts for the total measured  ${}^7\text{Li}$  yield. We point out that, strictly, both processes are coupled and should be treated simultaneously. For instance, the transfer to bound states of  ${}^{208}\text{Pb}$  could proceed through the continuum states by means of a multistep process. In practice, the inclusion of all possible intermediate couplings would require the solution of a large set of coupled

equations. We adopt a simpler approach, treating both processes separately. Test calculations revealed that couplings between the final transfer channels do not affect significantly the inclusive transfer cross sections.

### A. DWBA analysis

In this section we study the  ${}^7\text{Li}$  angular distribution coming from the one-neutron transfer leading to bound states of  ${}^{209}\text{Pb}$ . For this purpose, we use the DWBA amplitude. All calculations were performed for a bombarding energy of  $E_{c.m.} = 33.1$  MeV.

In the DWBA analysis, the entrance and exit channels are described by optical potentials, which are usually chosen to reproduce the elastic scattering cross sections in the respective channels. In particular, for the entrance channel we used the optical model potential OM-2 derived in the preceding section. For the exit channel, we adopted the  ${}^7\text{Li} + {}^{208}\text{Pb}$  optical potential obtained in Ref. [20], corrected by the mass of the target. In the present analysis, the post form of the DWBA amplitude was used. This involves the operator  $V_{[n-{}^7\text{Li}]} + U_{[{}^7\text{Li}, {}^{208}\text{Pb}]} - U_{[{}^7\text{Li}, {}^{209}\text{Pb}]}$ . The  $n-{}^7\text{Li}$  interaction was described in terms of a real Woods-Saxon potential, with the radius and diffuseness as those in the binding potential for  ${}^8\text{B}$  used in Ref. [22]. The potential depth was adjusted in order to reproduce the experimental binding energy. For the core-core interaction,  ${}^7\text{Li} + {}^{208}\text{Pb}$ , we used the optical potential from Ref. [20]. These potentials are shown in Table I.

The  ${}^8\text{Li}$  states considered in the calculation were described in the shell model, as it is shown in the Appendix. For the purpose of calculating transfer reactions, the relevant magnitudes are the coefficients of fractional parentage, which are defined as:

$$\text{CFP}(J|J_7, n\ell j) = \frac{\langle {}^8\text{Li}(J) || a_{n\ell j}^+ || {}^7\text{Li}(J_7) \rangle}{\sqrt{2J+1}}, \quad (1)$$

with reduced matrix element convention adopted in Ref. [26].

$$\text{CFP}(J|J_7, j) = \langle {}^8\text{Li}(J) || [a^+(j) \otimes |{}^7\text{Li}(J_7)\rangle]_J \rangle. \quad (2)$$

The relevant amplitudes for the ground state of  ${}^8\text{Li}$  are  $\text{CFP}(2^+|3/2^-, 1p_{3/2})$ ,  $\text{CFP}(2^+|3/2^-, 1p_{1/2})$ , and  $\text{CFP}(2^+|1/2^-, 1p_{3/2})$ . The first two components correspond to configurations with the  ${}^7\text{Li}$  in the ground state, while the last component corresponds to a configuration with  ${}^7\text{Li}$  in the first excited state. The values adopted in our calculations are derived in the Appendix and listed in Table II. We remark that, in our calculations, no excitation mechanism is considered between the  ${}^7\text{Li}$  ground state and  $1/2^-$  excited state. Therefore, the calculated  ${}^7\text{Li}$  in this excited state comes exclusively from the presence of this component in the  ${}^8\text{Li}$  ground state wave function.

In the present experiment, it was not possible to separate both states of  ${}^7\text{Li}$  in the measured cross sections. Then, in order to compare with the data, this component has to be included in our calculations. For the sake of clarity, we will use the names *elastic transfer* and *inelastic transfer*, in order to refer

TABLE II. Spectroscopic amplitudes for the  $\langle {}^8\text{Li}-{}^7\text{Li} \rangle$  overlaps.

Component			CFP( ${}^8\text{Li}$ )	
$J^\pi$	$J_7^\pi$	$n\ell j$	This work	Reference [23]
$2^+$	$3/2^-$	$1p_{3/2}$	0.943	1.025
	$3/2^-$	$1p_{1/2}$	0.471	0.366
	$1/2^-$	$1p_{3/2}$	-0.471	-0.535
$1^+$	$3/2^-$	$1p_{3/2}$	0.000	0.406
	$3/2^-$	$1p_{1/2}$	0.816	0.565
	$1/2^-$	$1p_{3/2}$	0.816	0.972
	$1/2^-$	$1p_{1/2}$	0.000	0.055

to the processes in which the outgoing  ${}^7\text{Li}$  remains in the ground state or the  $1/2^-$  excited state, respectively.

We note also that this experiment does not provide information on the final states populated in the  ${}^{209}\text{Pb}$  nucleus. Therefore, we have to include the transfer to all possible final states and the resulting cross sections need to be added incoherently. The  ${}^{209}\text{Pb}$  spectrum was described within a single-particle picture, in which the valence neutron is coupled to a  ${}^{208}\text{Pb}$  inert core. The bound state wave functions were generated with a Woods-Saxon potential, with standard parameters (see Table I) and spectroscopic factors taken from Ref. [27].

In Fig. 3, the experimental angular distributions for the total  ${}^7\text{Li}$  yield at  $E_{c.m.} = 32.9$  MeV (circles) and  $E_{c.m.} = 33.4$  MeV (squares) are shown, along with the calculations for the one-neutron transfer. These calculations are summed over all bound states of  ${}^{209}\text{Pb}$ . The DWBA results are represented by the dashed lines. The thin dashed lines correspond to the elastic and inelastic transfer, whereas the thick dashed line is the sum of both contributions. A comparison between the calculation and the data shows that the one-neutron transfer can account for most of the measured  ${}^7\text{Li}$  yield. However, there is still a clear underestimation of the data, suggesting that other channels contribute to the production of  ${}^7\text{Li}$  in this reaction.

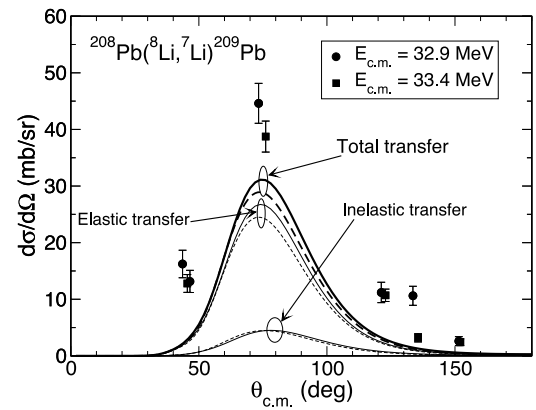


FIG. 3.  ${}^7\text{Li}$  angular distribution after  ${}^8\text{Li}$  one-neutron transfer leading to the bound states of  ${}^{209}\text{Pb}$ . The solid lines correspond to CCBA calculations, whereas the dashed lines are the DWBA results. Experimental data for the inclusive one-neutron removal are also shown.

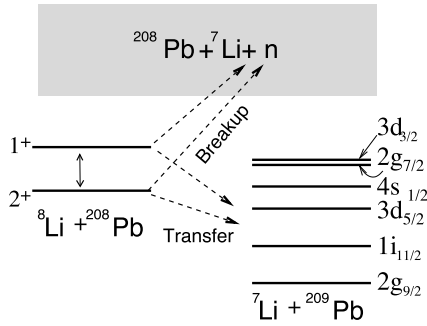


FIG. 4. Schematic representation of the couplings included in the CCBA calculations for one-neutron transfer and breakup.

### B. CCBA analysis

The first excited state in  $^8\text{Li}$  is strongly coupled to the ground state and, consequently, it could influence the transfer process. For instance, the projectile can be first excited before the valence neutron is transferred to the target. It is not obvious that this process is properly accounted for within a pure optical model description of the entrance channel, as it is assumed in the DWBA. As an improvement of the DWBA analysis, we have also performed calculations for the transfer cross sections using the CCBA approach. Here, we have used a more complete description of the entrance channel, by including explicitly the excited state of  $^8\text{Li}$ , along with the ground state. For the diagonal entrance optical potential we used the parameters CC. As in the DWBA analysis, the transfer coupling is treated in Born approximation. The relevant couplings are schematically represented in Fig. 4. Notice that the CCBA requires the spectroscopic factors for the overlaps  $\langle ^8\text{Li}(1_1^+) | ^7\text{Li}(3/2^-) \rangle$  and  $\langle ^8\text{Li}(1_1^+) | ^7\text{Li}(1/2^-) \rangle$ , which are also derived in the Appendix and listed in Table II.

In Fig. 5, we show the calculated energy- and angle-integrated cross sections to individual final states of the target. A clear dominance of the elastic transfer over the inelastic transfer is observed in all cases.

The  $^7\text{Li}$  angular distributions, obtained in this CCBA calculation, are compared in Fig. 3 with the DWBA results and the experimental data. The thin solid lines correspond to the elastic transfer and inelastic transfer contributions, as indicated by the labels. The thick lines correspond to the total transfer calculated in the CCBA (solid line) and DWBA (dashed line) approaches. We see that the DWBA and CCBA calculations give similar results. Since the values of  $B(E2)$  and  $\delta$  in  $^8\text{Li}$  are still quite uncertain from the experimental point of view, the small difference between DWBA and CCBA calculations indicates that reaction mechanisms in the entrance channel may not affect the transfer cross sections.

### IV. ONE-NEUTRON BREAKUP

Another process that can contribute to the production of  $^7\text{Li}$  is the breakup  $^8\text{Li}$  into  $^7\text{Li} + n$ , with the neutron being scattered instead of absorbed by the target. Physically, this process can be interpreted as single-particle excitations of  $^8\text{Li}$  into the  $^7\text{Li} + n$  continuum. As in the case of the transfer reaction, all possible final states should be considered. In order to make the number of states finite, the continuum is

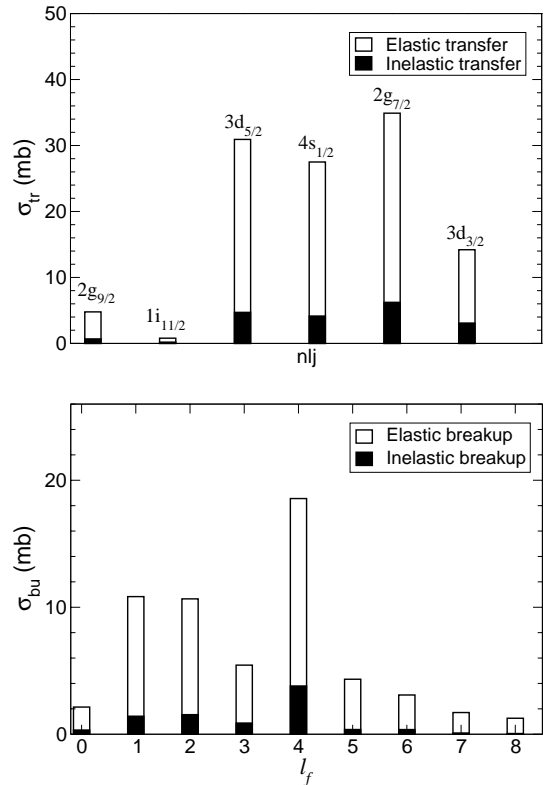


FIG. 5. Energy and angle integrated breakup cross sections for the transfer (upper panel) and breakup (lower panel) channels. In the former, the single-particle quantum numbers are indicated. In the latter, the abscissa correspond to the neutron- $^{208}\text{Pb}$  relative angular momentum.

commonly discretized into a set of energy bins and only the relevant partial waves for the  $n$ - $^7\text{Li}$  relative motion are retained. Then, a coupled-channels calculation is performed within this truncated space. This procedure, usually referred to as continuum discretized coupled channels (CDCC), has been successfully used to study the elastic and breakup channels of many reactions involving weakly bound nuclei. However, for the reaction under study, this approach presents some disadvantages. The nonzero spin of the core makes the number of continuum bins very large, even if a small number of partial waves are retained. Another limitation is that, besides the coupling to the continuum states, it would be also necessary to consider in the calculations the excitation to the  $1_1^+$  excited state of  $^8\text{Li}$ , which we have shown to have a relevant role in the description of the entrance channel. The coupling to this state is better treated within a collective picture of the  $^8\text{Li}$  nucleus which, in practice, is implemented by using a deformed potential for the entrance channel. By contrast, continuum states are better treated within a single-particle picture. However, it is not obvious how to combine both descriptions in the same partition. Due to these difficulties, we have adopted a different approach, in which the  $^8\text{Li}$  breakup is treated as a one-neutron transfer to the continuum states of the target, as illustrated schematically in Fig. 4. Note that, in this way, the breakup channels are strictly orthogonal to the transfer channels and so overcounting is avoided.

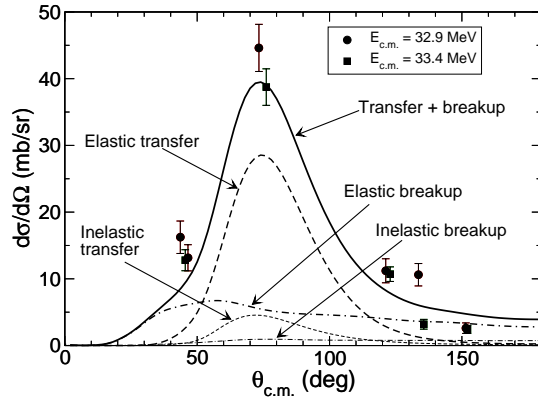


FIG. 6.  ${}^7\text{Li}$  angular distribution after  ${}^8\text{Li}$  breakup/transfer. The lines show the result of our CCBA calculations, as described in the text.

As in the conventional CDCC approach, we perform a discretization of the  ${}^{208}\text{Pb}-n$  two-body continuum into a set of energy bins. For each partial wave, we considered  $N=3$  bins of equal width, up to  $\epsilon_{\text{max}}=6$  MeV. In connection with the analysis of the elastic scattering performed in the preceding section, we adopt a two-state model for the entrance channel, comprising the  $2_1^+$  and  $1_1^+$  states of  ${}^8\text{Li}$ . As in the case of bound states, we treat the transfer in Born approximation. Note that, within this procedure, the breakup amplitude is formally equivalent to a CCBA calculation, in which the final states are continuum bins instead of bound states. Therefore, this method provides a description of the one-neutron transfer and breakup processes within a common formalism. For consistency, we used the same ingredients as for the CCBA calculations discussed in the preceding section. In particular, the  ${}^{208}\text{Pb}-n$  continuum states are generated with the potential of Table I.

In these circumstances, the breakup of  ${}^8\text{Li}$  may leave the outgoing  ${}^7\text{Li}$  in the ground or the excited state. In order to distinguish between the two situations, we will use the names of *elastic* and *inelastic breakup*.

The calculated angle- and energy-integrated breakup cross sections are schematically depicted in the lower panel of Fig. 5 as a function of the relative angular momentum between the  ${}^{208}\text{Pb}$  and the transferred neutron,  $\ell_f$ . It is interesting to note that the breakup is maximum for  $\ell_f=4$  and then decays gradually for higher partial waves. As observed in Fig. 5, a good convergence of the breakup cross section is achieved with a few partial waves ( $\ell_f \approx 8$ ). Note that, despite the formal similitude between the DWBA and CCBA expressions for transfer and breakup, the calculation is much more demanding in the latter case, due to the long range of the continuum (or bin) wave functions. For instance, while transfer calculations converge integrating the coupled equations up to  $R_m=60$  fm and  $L_{\text{max}}=60$ , the breakup calculations require typically  $R_{\text{max}} \approx 200$  fm and  $L_{\text{max}} \approx 150$ .

The calculated angular distributions for the elastic and inelastic breakup are shown in Fig. 6. The elastic (inelastic) breakup is given by the thick (thin) dotted-dashed line. For comparison, the CCBA elastic and inelastic transfer cross sections of Fig. 3 have also been plotted in this figure.

The sum of the transfer and breakup distributions (including both the elastic and inelastic components) is given by the thick solid line. We find a very good agreement with the experimental distribution, in both shape and magnitude. By comparison of the relative magnitudes of the different processes, we observe that the dominant mechanism leading to one-neutron removal from the projectile is the transfer to the bound states of the target. According to the present calculations, this process accounts for about 70% of the total  ${}^7\text{Li}$  cross section. This result extends the conclusions outlined in Ref. [28], where the single-neutron transfer was also identified as the most prominent reaction mechanism in the scattering of  ${}^8\text{Li}$  by light targets ( ${}^9\text{Be}$  and  ${}^{12}\text{C}$ ). As done in that work, we interpret this result as a consequence of the small binding energy of the last neutron in  ${}^8\text{Li}$  and the positive  $Q$  values (which facilitates momentum matching) for these reactions.

Apart from the clear dominance of the transfer cross section over the breakup cross section, our calculations indicate a rather different angular shape for these two mechanisms. While the transfer angular distribution exhibits a symmetrical shape, peaked around the rainbow angle ( $\approx 75^\circ$ ), the breakup shows a broad and asymmetrical distribution. We interpret the difference as follows. The transition probability depends crucially on the overlap of initial and final states, in the region where the interaction potential is relevant. The spatial confinement of bound states, together with the matching conditions, makes the transfer effective on a relatively narrow window of angular momenta. On the other side, absorption of the imaginary potentials suppresses the transfer probability in collisions if the projectile and target come very close to each other. These two effects tend to favor the transfer for grazing collisions, giving rise to an angular distribution peaked around the grazing angle. By contrast, the infinite extension of continuum wave functions permits the breakup at large projectile target separations. For small impact parameters, breakup can occur to configurations where the fragments are well apart and where the particles can survive without being absorbed, even if the center of mass corresponds to a close collision. This implies that breakup can be important at small partial waves, where the transfer is likely to be suppressed by the nuclear absorption. Also, we expect the Coulomb field to induce breakup at large partial waves, where transfer is suppressed due to the exponential decay of the bound states. In addition, breakup can occur for many different energy and angular momentum configurations, and so the total angular distribution should be understood as a superposition of many different final states of energy and angular momentum, each having a different angular shape. In conclusion, we expect the breakup process to be effective on a wider range of partial waves, as compared to the transfer process, and this could explain its broader angular distribution. This different nature between the transfer and breakup mechanisms will be more evident at low energies where Coulomb effects become more important in relation to nuclear effects.

## V. CRC CALCULATIONS

The relatively large transfer/breakup cross section observed in this reaction evidences a strong coupling of these

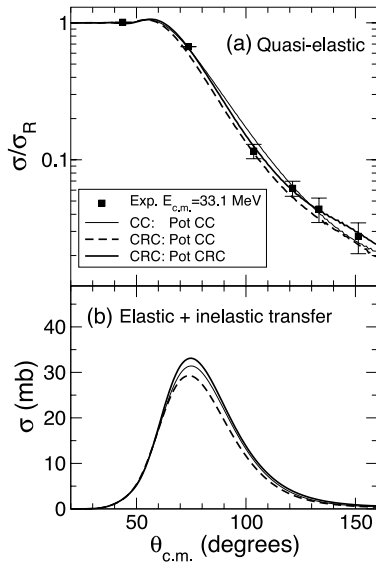


FIG. 7. Coupled reaction channels calculations for the quasielastic (a) and single-neutron transfer (b) cross sections, using the optical potentials “CC” and “CRC” for the entrance channel.

channels with the elastic channel. In these situations, a proper treatment of the reaction requires a joint analysis of elastic and rearrangements channels. However, the DWBA and CCBA approaches calculate the transfer cross section in Born approximation and assume that all effects on the elastics coming from these channels can be included in an effective way in the entrance optical potential. We have examined the accuracy of these assumptions for the present reaction by performing a coupled reaction channels (CRC) calculation, in which the transfer couplings are treated beyond the Born approximation and, hence, can modify the elastic distribution. At this stage, we do not include couplings among the final states themselves, in order to make the calculations more feasible. For the diagonal part of the optical potential in the entrance channel we took the parameters CC.

The results of these calculations are shown in Fig. 7. The upper and lower panels correspond, respectively, to the quasielastic and transfer angular distributions. The thin solid line in the upper panel shows our previous CC calculation for the quasielastic distribution. Analogously, the thin solid line in the bottom panel corresponds to the transfer distribution, obtained in the CCBA scheme. When transfer back couplings are included, an overall reduction of the elastic and transfer distributions is observed, as shown by the dashed lines. In order to restore the description of the elastic channel, we decreased the imaginary diffuseness of the entrance optical potential from  $a_i=0.60$  fm to  $a_i=0.55$  fm, leading to a good agreement with the experiment (thick solid line). Basically, the effect of decreasing the imaginary diffuseness is to reduce the absorption in the entrance channel. Interestingly, this change increases the transfer cross section giving a distribution very close to the original CCBA distribution. It is worth noting that starting with the parameters of the potential OM-2 very similar results were obtained. As before, we found that the optical potential used to describe the en-

trance channel in the CRC calculation is less absorptive than the original potential.

We note, however, that the calculations presented correspond just to a truncated CRC calculation in which only transfer channels are properly coupled to the elastic channel. A full CRC calculation would require the simultaneous inclusion of breakup and transfer channels. Moreover, the final states of the target (bound and unbound) should be coupled together. This calculation is numerically very demanding and it is probably not justified given the uncertainties of the present data. Moreover, we expect less influence of the breakup channels as compared with the transfer channels, since the cross section for the former is considerably smaller.

## VI. SUMMARY AND CONCLUSIONS

In this work, we have performed an analysis of the elastic and one-neutron removal channels for the scattering of  $^8\text{Li}$  on lead, at energies around the Coulomb barrier. The measured quasielastic scattering angular distributions can be accurately reproduced by using a conventional Woods-Saxon optical potential. There are ambiguities in the determination of the parameters of the optical potentials. However, all the potentials that fit the elastic data are strongly absorptive, having either a very deep imaginary potential or a very diffuse one.

In order to disentangle the elastic and inelastic contributions to the quasielastic data, we have performed a coupled-channel calculation that includes explicitly the ground and excited state of  $^8\text{Li}$  in the entrance channel. This calculation shows that a significant fraction of the measured  $^8\text{Li}$  at  $E_{c.m.}=33.1$  MeV in the large angle region is in the  $1_1^+$  excited state.

We have investigated the reaction channels that lead to  $^7\text{Li}$ : transfer channels, populating the bound states in  $^{209}\text{Pb}$ , or breakup channels, leading to a three-body final state with  $^7\text{Li}$ ,  $^{208}\text{Pb}$ , and a neutron. We have described the breakup channels discretizing the  $n$ - $^{208}\text{Pb}$  continuum into energy bins and treating the breakup as a transfer of the valence neutron to these continuum bins. One of the most striking conclusions of this work is that 70% of the one-removal cross section comes from transfer. Also, we find that the summed contribution of the calculated transfer and breakup is in good agreement with the experimental angular distribution for the inclusive  $^7\text{Li}$  cross section. Interestingly, the value of the transfer and breakup cross sections are not affected by the uncertainties in the optical potential.

We have also studied the effect of the transfer channels on the elastic cross sections by performing a CRC calculation that couples simultaneously the elastic, inelastic, and transfer channels. These CRC calculations reveal that the single-neutron transfer produces a significant depletion of the elastic angular distribution. We find also that a less absorptive potential is required when these transfer channels are included. This indicates that reaction channels leading to  $^7\text{Li}$  (transfer and breakup) play an important role in collisions of  $^8\text{Li}$  on  $^{208}\text{Pb}$ . However, other reaction channels should be responsible for the still large absorption which is required in the CRC calculation.

One of these channels could be the transfer/breakup leading to  $\alpha$  particles, also detected in this experiment. No attempt has been made in this work to calculate the  ${}^4\text{He}$  angular distribution, reported in Ref. [16]. In that work, the  ${}^4\text{He}$  yield is interpreted as coming from the sequential breakup:  ${}^8\text{Li} \rightarrow {}^7\text{Li} + n$ , followed by  ${}^7\text{Li} \rightarrow \alpha + t$ . Another process that can contribute is the direct breakup of  ${}^8\text{Li}$  into the three-body system  $\alpha + t + n$ . Furthermore, other experiments have observed very energetic  $\alpha$  particles in  ${}^8\text{Li}$ -induced reactions with light targets ( ${}^1\text{H}$ ,  ${}^9\text{Be}$ ,  ${}^{12}\text{C}$ ) at  $E_{lab} = 14$  MeV. Their angular distribution seems to be indicative of a compound-nucleus fusion evaporation mechanism rather than a direct mechanism [28]. More exclusive measurements for the present reaction in future experiments would be desirable in order to provide a better understanding of the relevant reaction mechanisms responsible for the production of  $\alpha$  particles.

### ACKNOWLEDGMENTS

We are grateful to I. J. Thompson, R. Johnson, A. Mukhamedzhanov, and N. Timofeyuk for useful discussions. This work was partially supported by Fundação para a Ciência e a Tecnologia (FCT) of Portugal, under Grant No. POCTI/36282/99, the Ministerio de Ciencia y Tecnología (Spain), Project No. FPA2002-04181-C04-04 and the CONACYT (Mexico). A.M.M. acknowledges a grant from the FCT.

### APPENDIX SPECTROSCOPIC AMPLITUDES FOR $\langle {}^8\text{Li} | {}^7\text{Li} \rangle$

The CCBA and DWBA calculations performed in this work require the spectroscopic amplitudes which correspond to the coefficients of the expansion of the  ${}^8\text{Li}$  wave function in terms of  $|{}^7\text{Li}\rangle \otimes |n\rangle$  product states. To perform this evaluation we have made the following assumptions.

(i) The relevant states of  ${}^8\text{Li}$  and  ${}^7\text{Li}$  are described in the shell model as  $(1p)^4$  and  $(1p)^3$  configurations, respectively, outside a closed  $(1s)^4$  shell.

(ii) Wigner supermultiplet scheme is considered to be adequate to label completely these states, which then are fully characterized by the Young tableau describing the spacial symmetry  $Y$ , the orbital angular momentum of the nucleons  $L$ , the spin  $S$ , the isospin  $T$ , and the total angular momentum

$J$ . This description is adequate for nuclei in the first half of the  $p$  shell.

The relevant states of  ${}^7\text{Li}$  are characterized by the maximum spatial symmetry, corresponding to the Young tableau  $Y = [3]$ . This allows the values  $S = 1/2$ ,  $T = 1/2$ , and  $L = 1, 3$ . The  $3/2^-$  ground and  $1/2^-$  first excited state of  ${}^7\text{Li}$  form a doublet with  $L = 1$  and  $S = 1/2$ . The  $3/2^-$  and  $5/2^-$  resonances form a doublet with  $L = 3$  and  $S = 1/2$ .

The relevant states of  ${}^8\text{Li}$  are characterized by the maximum spatial symmetry which, for three neutrons and a proton, is given by the Young tableau  $Y = [3, 1]$ . This allows the values  $T = 1$ ,  $S = 0, 1$ , and  $L = 1, 2, 3$ . The states with higher spin and lower orbital angular momentum are lower in energy. So, the ground state  $J = 2^+$  and the first excited state  $J = 1^+$  belong to a triplet with  $L = 1$  and  $S = 1$ . This argument is in agreement with theoretical calculations [29,30] which show that  $L = S = 1$  configurations are dominant for the ground state and for the first excited state.

The  ${}^7\text{Li}$  states couple to the valence neutron, characterized by the angular momenta  $\ell = 1$ ,  $s = 1/2$ , and  $j = 3/2, 1/2$  to give  ${}^8\text{Li}$ . The CFP can be transformed from the  $j$ - $j$  to the  $L$ - $S$  coupling scheme:

$$\begin{aligned} \text{CFP}((LS)J|(L_7S_7)J_7; \ell sj) \\ = \begin{Bmatrix} L_7 & \ell & L \\ S_7 & s & S \\ J_7 & j & J \end{Bmatrix} \hat{J}_7 \hat{j} \hat{L} \hat{S} \text{CFP}(LS|L_7\ell, S_7s). \end{aligned} \quad (\text{A1})$$

The values of the coefficients  $\text{CFP}(LS|L_7\ell, S_7s)$  can be explicitly evaluated in our case, by expanding the wave functions of  ${}^8\text{Li}$  and  ${}^7\text{Li}$  in terms of products of nucleon wave functions. Thus, we obtain  $\text{CFP}(11|11, 1/21/2) = \sqrt{4/3}$ .

The calculated CFP's are listed in Table II, and compared with a recent theoretical prediction [23]. According to theoretical calculations (see, for instance, Ref. [29]) this is a very good approximation for the ground state (the  $L = 1, S = 1$  configuration appears to be around 80%). For the excited state, there is a significant contribution coming from the components  $L = 2, S = 1$  and  $L = 1, S = 0$ . However, as the  ${}^8\text{Li}$  excited state only participates in the transfer by means of two step processes, a strong sensitivity of the results with respect to the description of this state is not expected.

- 
- [1] M.S. Hussein, M.P. Pato, L.F. Canto, and R. Donangelo, Phys. Rev. C **46**, 377 (1992).  
 [2] M.S. Hussein and A.F.R. de Toledo Piza, Phys. Rev. Lett. **72**, 2693 (1994).  
 [3] C.H. Dasso and A. Vitturi, Phys. Rev. C **50**, R12 (1994).  
 [4] C.H. Dasso, J.L. Guisado, S.M. Lenzi, and A. Vitturi, Nucl. Phys. **A597**, 473 (1996).  
 [5] K. Yabana, Prog. Theor. Phys. **97**, 437 (1997).  
 [6] M. Trotta *et al.*, Phys. Rev. Lett. **84**, 2342 (2000).  
 [7] A. Díaz-Torres and I.J. Thompson, Phys. Rev. C **65**, 024606 (2002).  
 [8] C. Signorini, Eur. Phys. J. A **13**, 129 (2002).  
 [9] D.J. Hinde, M. Dasgupta, B.R. Fulton, C.R. Morton, R.J. Wooliscroft, A.C. Berriman, and K. Hagino, Phys. Rev. Lett. **89**, 272701 (2002).  
 [10] C. Signorini, Nucl. Phys. **A693**, 190 (2001).  
 [11] E.F. Aguilera *et al.*, Phys. Rev. Lett. **84**, 5058 (2000).  
 [12] E.F. Aguilera *et al.*, Phys. Rev. C **63**, 061603 (2001).  
 [13] B.T. Kim, W.Y. So, S.W. Hong, and T. Udagawa, Phys. Rev. C **65**, 044616 (2002).  
 [14] G.R. Kelly *et al.*, Phys. Rev. C **63**, 024601 (2001).  
 [15] A. Szantos de Toledo *et al.*, *Proceedings for the XXV Reunión*

- de trabalhos de Física Nuclear Brasileira, São Pedro, São Paulo, Brazil, 2002* [Braz. J. Phys. **33**(2) (2002)].
- [16] J.J. Kolata *et al.*, Phys. Rev. C **65**, 054616 (2002).
- [17] R. Chatterjee, P. Banerjee, and R. Shyam, Nucl. Phys. **A675**, 477 (2000).
- [18] R. Chatterjee and R. Shyam, Phys. Rev. C **66**, 061601 (2002).
- [19] A. Bonaccorso and D.M. Brink, Phys. Rev. C **38**, 1776 (1988).
- [20] I. Martel, *et al.*, Nucl. Phys. **A582**, 357 (1995).
- [21] I.J. Thompson, Comput. Phys. Rep. **7**, 167 (1988).
- [22] H. Esbensen and G.F. Bertsch, Nucl. Phys. **A600**, 37 (1996).
- [23] N. K. Timofeyuk (private communication); N.K. Timofeyuk, Nucl. Phys. **A632**, 19 (1998).
- [24] A. M. Moro, R. Crespo, H. García-Martínez, E. F. Aguilera, E. Martínez-Quiroz, J. Gómez-Camacho, and F. M. Nunes, *Proceedings of the XXVI Symposium on Nuclear Physics, Taxco, Mexico*, edited by Sociedad Mexicana de Física [Rev. Mex. Fis. (2003)].
- [25] R.J. Smith, J.J. Kolata, K. Lamkin, A. Morsad, F.D. Becchetti, J.A. Brown, W.Z. Liu, J.W. Janecke, D.A. Roberts, and R.E. Warner, Phys. Rev. C **43**, 2346 (1991).
- [26] I. Talmi, *Simple Models of Complex Nuclei: The Shell Model and Interacting Boson Model* (Gordon and Breach, New York, 1993).
- [27] I. J. Thompson (private communication); J.S. Lilley, M.A. Nagarajan, D.W. Banes, B.R. Fulton, and I.J. Thompson, Nucl. Phys. **A4632**, 170 (1987).
- [28] F.D. Becchetti, W.Z. Liu, D.A. Roberts, J.W. Janecke, J.J. Kolata, A. Morsad, X.J. Kong, and R.E. Warner, Phys. Rev. C **40**, R1104 (1989).
- [29] R.B. Wiringa, S.C. Pieper, J. Carlson, and V.R. Pandharipande, Phys. Rev. C **62**, 014001 (2000).
- [30] L.V. Grigorenko, B.V. Danilin, V.D. Efros, N.B. Shul'gina, and M.V. Zhukov, Phys. Rev. C **57**, R2099 (1998).